AIAA JOURNAL
Vol. 44, No. 7, July 2006

Unsteady Plasma Actuators for Separation Control of Low-Pressure Turbine Blades

Junhui Huang,* Thomas C. Corke,† and Flint O. Thomas‡
University of Notre Dame, Notre Dame, Indiana 46556

DOI: 10.2514/1.19243

This is a continuation of our work on the use of single dielectric barrier plasma actuators for controlling flow separation on turbine blades in the low-pressure turbine stage at low Reynolds numbers typical of high-altitude cruise. This used a linear cascade of Pratt & Whitney "PakB" shaped blades to provide generic low-pressure turbine conditions. The flow over one of the blades was documented through surface pressure, laser-Doppler velocimetry, and hot-wire measurements. These were used to define the location and size of the separated flow region on the suction side of the blade. Both steady and unsteady plasma actuators were implemented and found to be effective in separation control. For the unsteady actuators, there was an optimum excitation frequency to reattach the flow that corresponded to a Strouhal number, based on the length of the separated zone and the local freestream velocity, equal to unity. The unsteady actuator was more effective than the steady actuator in reattaching the flow while also requiring less power. It was suggested by the experimental results that the mechanism for the steady actuators was turbulence tripping, whereas the mechanism for the unsteady actuators was to generate a train of spanwise structures that promoted mixing.

Nomenclature

C_p	=	pressure coefficient, $=(p - p_\infty)/(\frac{1}{2}\rho U_\infty^2)$
C_x	=	axial chord length
$\boldsymbol{E}$	=	electric field vector
e	=	elementary charge
$\boldsymbol{f}$	=	body force generated by plasma
f	=	excitation frequency of unsteady plasma actuator
k	=	Boltzmann's Constant
L_{sep}	=	length of separation region
n_0	=	plasma density
p	=	static pressure
p_∞	=	static pressure in the freestream
q	=	dynamic pressure
Re_c	=	Reynolds number based on axial chord length and freestream velocity
T_{control}	=	time period for unsteady operation, $=1/f_{\text{control}}$
T_{signal}	=	actuator on time period for unsteady operation
U_∞	=	freestream velocity
$U_{\text{midchannel}}$	=	local freestream velocity in blade passageway
u, v, w	=	velocity components
u', v', w'	=	rms velocities
x, y	=	axial coordinates
β	=	plasma duty cycle, $=T_{\text{signal}}/T_{\text{control}}$
ϵ_0	=	permittivity of free-space
λ_D	=	Debye length
ρ	=	density of air
ϕ	=	electric potential

I. Introduction

GAS-TURBINE engines are usually designed for peak performance at high Reynolds number conditions, such as at takeoff and landing. However, during high-altitude cruise, the operating Reynolds number for the low-pressure turbine (LPT) can drop below 25,000 due to the low air density. The optimally designed engines for high Reynolds number conditions may perform poorly under various off-design conditions and suffer a substantial loss of engine efficiency. Sharma [1] indicated a nearly 300% rise in the loss coefficient at Reynolds numbers below 95,000 compared with that at higher Reynolds numbers. The high total pressure loss at low Reynolds numbers was found to be primarily associated with a laminar flow separation over the trailing half of the LPT blade suction surface.

The solution to this problem is to apply a control method to eliminate the flow separation that occurs on the LPT blade at low Reynolds numbers. Although passive methods for avoiding laminar separation might be advisable, such standard methods as altering the blade shape or using boundary layer trips or vortex generators would produce a parasitic effect on the engine performance when not needed at higher Reynolds number conditions. In addition, from an engine design standpoint, a lower number of more highly loaded stages, which would also have a greater potential for flow separation, is more desirable to minimize engine cost, weight, and length. Therefore, on-demand active separation control provides the best opportunity to achieve an overall improvement in engine performance and will likely lead to enhanced designs with a lower part count, size, and weight.

The potential this offers has motivated work on controlling flow separation over LPT blades. Byerley et al. [2] used passive Gurney flaps to control laminar separation on a linear cascade of seven "Langston" blades. Five different sizes of Gurney flaps were tested. The largest and second largest Gurney flaps completely eliminated separation at the lowest Reynolds number. However, it was found that the Gurney flaps increased the loss coefficient when the Reynolds number was high enough that separation was not present. Lake et al. [3], and Bons et al. [4–6] used a linear cascade of "PakB" blades to simulate the pressure gradient for a generic LPT blade row. The PakB geometry was designed by Pratt & Whitney to produce a pressure distribution on blades in a linear cascade that was comparable to those in the gas-turbine engines. Lake et al. [3] applied spherical dimples to the surface of the blades to passively force flow reattachment. Bons et al. [4–6] and Volino [7] used steady and pulsed blowing of air through angled holes in the blade surface. Their approaches aimed to produce streamwise vortices like those used to prevent flow separation on aircraft wings and in diffusers.

Our approach to separation control over the LPT blades is based on the use of single dielectric barrier (SDB) plasma actuators [8,9].

Received 30 July 2005; revision received 20 February 2006; accepted for publication 21 February 2006.

*Graduate Assistant, Center for Flow Physics and Control, Aerospace and Mechanical Engineering Department.

†Clark Chair Professor, Center for Flow Physics and Control, Aerospace and Mechanical Engineering Department. Associate Fellow AIAA.

‡Professor, Center for Flow Physics and Control, Aerospace and Mechanical Engineering Department. Associate Fellow AIAA

These actuators consist of electrode pairs separated by a thin dielectric insulator that is located on the surface of the blades. A high voltage ac is supplied to the electrodes that causes the air in their vicinity to weakly ionize. The ionized air (plasma) in the presence of the electric field gradient produced by the electrodes results in a body force vector acting on the external flow that can induce steady or unsteady velocity components. Numerical simulations (Orlov et al. [10]) of the electric field, body force, and induced velocities have led to optimized designs. Descriptions of our actuator designs are presented by Corke and Matlis [11] and Post [12].

Plasma actuators have drawn considerable attention and been used in many applications in recent years. Matlis [13] used an azimuthal array of plasma actuators to excite oblique waves with a prescribed amplitude, frequency, and azimuthal wave number near the tip of a sharp cone at Mach 3.5. Corke et al. [14] used the plasma actuators on a NACA-0009 airfoil to produce lift enhancement similar to plane trailing-edge flaps. Wilkinson [15] tried to simulate an oscillating wall by means of plasma arrays. Enloe et al. [16,17] conducted optical, electrical, and thrust measurements to understand the physics of plasma actuators. Post and Corke [18] and Corke et al. [19] used plasma actuators to control leading-edge separation and to increase $C_{l_{\max}}$ and α_s on steady airfoils. Post [20] used these on the leading edge of oscillating airfoils to control the dynamic stall vortex. Thomas et al. [21] demonstrated bluff body separation control for the purpose of landing gear noise reduction. Hultgren and Ashpis [22] used an array of plasma actuators to affect separation in a wind-tunnel section that was designed to produce the same streamwise pressure gradient as on the suction surface of a PakB blade. An overview of various applications of SDB plasma actuators was given by Corke and Post [23].

The object of our research was to use the SDB plasma actuators to improve the performance of LPT stage of gas-turbine engines by actively controlling flow separation that occurs over the suction surface of the blades at low Reynolds numbers consistent with high-altitude cruise. Documentation of the effect of the actuators involves surface pressure measurements on the blades and velocity profiles obtained using hot-wire and laser-Doppler anemometers. The improvements in the loss coefficient are then determined.

II. Experimental Setup

A specially designed linear cascade wind tunnel was built for the experiments. A schematic of the tunnel is shown in Fig. 1. The freestream turbulence intensity upstream of the cascade was $u'/U_\infty = 0.08\%$ ($0000'$ denotes an rms value). This included all frequencies in a band from 1 Hz to 10 kHz.

A straight section following the contraction gives access to place turbulence generating devices upstream of the cascade. The inlet to the cascade has a 36.5 in. (0.93 m) square cross-section dimension. The linear cascade consists of nine PakB blades which span a 95 deg turn. Trailing-edge splitter plates ("tail boards") were attached to the trailing edges of the most outboard and inboard blades to aid the flow in negotiating the turn and to maintain the correct pressure gradient on the blades. The angles of the tail boards were adjusted so that at high chord Reynolds numbers the pressure distribution on the blades agreed with high Reynolds number (Euler) calculations.[§] Surface pressure measurements made one-third of a blade span on either side of the center-span location verified the two dimensionality of the flow through the cascade [9].

The top wall of the cascade section and the side walls of the straight section downstream of the cascade are made of clear Lexan, with plate glass inserts where necessary, to allow optical access for laser-Doppler velocimetry (LDV) measurements and flow visualization. Photographs of the cascade section are shown in Fig. 2. The left photograph is a view on top of the cascade that also shows the LDV optical head holder and wake traversing systems. The right photograph shows a side view of blades and traversed pitot probe used in wake measurements.

The PakB blades are cast in an acrylic polymer in a numerically machined aluminum mold. The chord dimension is 7 in. (17.78 cm).

[§]Romeo, S., private communication, 2002.

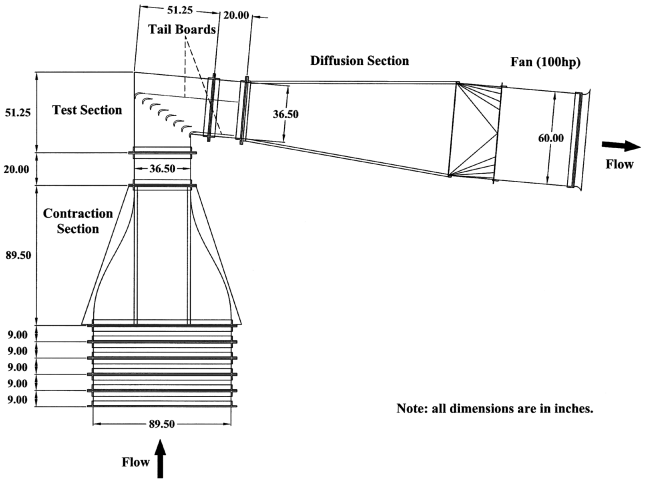

Fig. 1 Schematic drawing of the linear cascade wind tunnel used for the experiments.

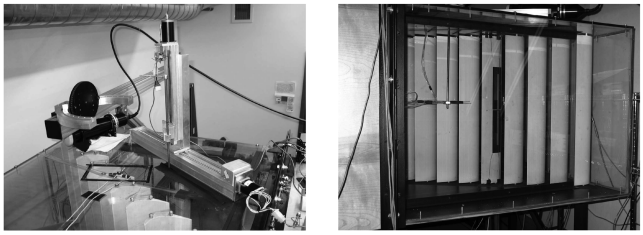

Fig. 2 Photographs of the linear cascade section.

These are designed to span the full height of the cascade section less a 0.25 in. (0.64 cm) gap at each end. The blades have threaded inserts that are molded into the blades ends to accept mounting bolts. The mounting bolts pass through the top and bottom walls of the cascade section. Round spacer washers take up the gap between the blade ends and the top and bottom walls.

The center blade is molded with 40 surface pressure ports. The diameter of each of the ports is 0.0625 in. (1.6 mm). A majority of the taps are on the suction side of the blade, with a special concentration in the region of $0.5 \leq x/C_x \leq 1.0$, where the flow is expected to separate at lower Reynolds numbers. The pressure taps are located at the midspan location of the blade and are distributed in the chordwise direction. A smaller number of taps are located at other spanwise positions and are used only early in the study to confirm the two dimensionality of the blade pressure distribution. The surface pressure is transmitted through 0.0625 in. (1.6 mm) diameter tubulations that are molded inside the blade and exit through the bottom end. These turbulations are connected to a scanning pressure valve (Scanivalve JS4-48) that multiplexed each pressure port to a single differential pressure transducer. The uncertainty of the pressure measurements was evaluated using a method proposed by Figliola and Beasley [24] and was calculated to be 1.52% of the measured pressure. This includes the digital quantization and calibration errors.

The boundary layer profiles over the surface of the blades was measured using LDV and hot wires. An aerometric fiber optic LDV system was operating in one-component back-scatter mode to measure the streamwise velocity u. Frequency shifting was used to unambiguously resolve the flow direction. The LDV transceiver was mounted on a specially designed rotary head, shown in the left photograph in Fig. 2, that was connected to a computer controlled traverse table. The rotary head allowed the transceiver to be manipulated to align the probe volume parallel to the local blade surface. The accuracy of the movement of the traverse table was 0.4 μm. Wind-tunnel seeding was performed at the tunnel inlet with a TSI, Inc., droplet generator (model 9307) using olive oil. The mean particle size was measured to be 1 μm.

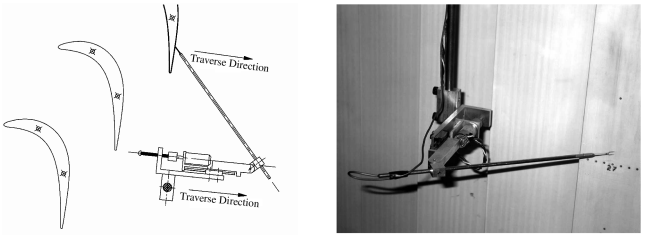

Fig. 3 Hot-wire probe mounted on a minitraverse for boundary layer surveys.

The hot-wire measurements were used to provide a check on the accuracy of the LDV measurements, except in regions of flow reversal, and for power spectrum measurements of velocity fluctuations. The hot-wire probe was attached to a minitraverse system, which was mounted inside the test section, downstream from the PakB cascade. A MicroMo, Inc., stepper motor was used to drive a linear rail which held the hot-wire probe. The linear rail was aligned perpendicular to the local blade surface. The accuracy of the minitraverse system is 50 μm. Figure 3 shows a schematic and a photograph of the minitraverse system with mounted hot-wire probe.

Bulk flow instrumentation consisted of a total-static pitot tube and a Velmex two-dimensional traverse system, shown in the right photograph in Fig. 2. A 15-in.-long slot was cut into the top wall of the test section at one axial chord length downstream from the trailing-edge of the center blade. The Velmex traverse system was located on the top wall of the test section. The pitot tube was mounted on the traverse system by a $\frac{3}{8}$-in.-diam iron rod. The slot was parallel to the trailing-edge of the cascade and allowed the measurement of the wakes of two consecutive blades.

Flow visualization was conducted by illuminating a stream of tracer particles with a laser light sheet. The particles were generated using a TSI droplet generator with olive oil. They were introduced into the wind tunnel at the tunnel inlet. The density of the particles and the location of injection were carefully adjusted so that an appropriate amount of particles passed through the cascade passages surrounding the center blade. The laser sheet was projected into the cascade from the trailing-edge at the height of the particle stream. In the case of unsteady actuator pulsing, in order to capture the dynamic flow effect, a laser chopper was inserted between the laser sheet projector and the laser generator. The chopper frequency was set to be close to the unsteady actuator frequency to slow down the visual motion of the flow. The visualized flow was recorded using a Sony DCR-TRV740 digital camcorder that viewed the flow from the top of the of the cascade section.

III. Experimental Results

A. Baseline Conditions

Baseline flow measurements were made in our previous work [8]. These documented the effects of the chord Reynolds number and turbulence intensity on the locations of flow separation and reattachment on the suction side of the blade. This was documented through the surface pressure coefficients and the boundary layer profiles. An example of these results is shown in Fig. 4. This shows the pressure coefficient distribution around the blade at the midspan location. The blade pressure coefficient is defined as $C_p \equiv (p - p_\infty)/q$, where p is the blade surface pressure $q = \frac{1}{2}\rho U_\infty^2$ and U_∞ and p_∞ are measured in the straight section upstream of the cascade. Figure 4 documents the effect of the blade chord Reynolds number for the range $10,000 \leq Re_c \leq 100,000$ and the lowest freestream turbulence intensity of $u'/U_\infty = 0.08\%$. The solid curve corresponds to the computed pressure distribution based on an Euler (inviscid) code.[‖] The computations are equivalent to an infinite Reynolds number and, therefore, should indicate the C_p distribution without flow separation. Deviations between the measured distributions and the Euler distribution indicate the region of flow

[‖]Romeo, S., private communication, 2002.

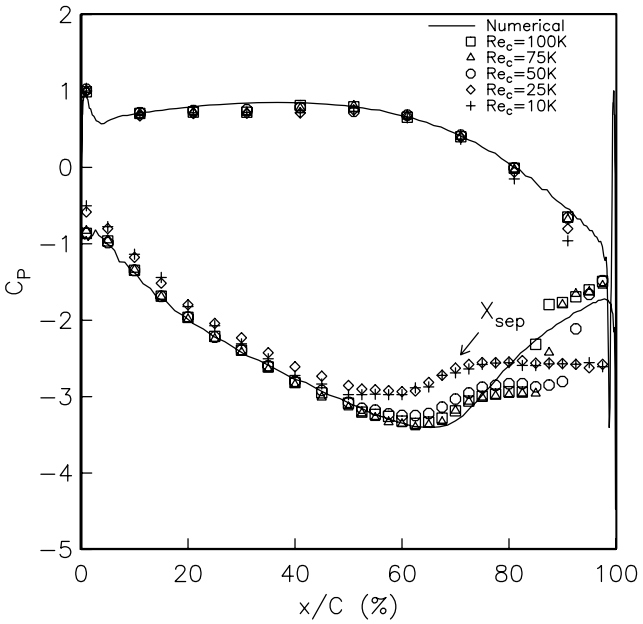

Fig. 4 Pressure coefficient distributions for different Reynolds numbers for the lowest (0.08%) freestream turbulence intensity, and comparison to Euler simulation (Romeo, private communication).

separation. This is observed to occur only on the aft potion of the suction (negative C_p) side of the blade.

The flow separation location is defined as the the point of inflexion in the region of increasing C_p near the trailing edge of the suction side of the blade. In Fig. 4, this point occurs near $x/C_x \approx 72\%$ and has been indicated as X_{sep}. The reattachment location is defined as the point where the C_p jumps from the nearly constant value that is the hallmark of a separated region and begins to follow the inviscid distribution close to the trailing edge. At $Re_c = 100,000$, this occurs at $x/C \simeq 0.85$. For Re_c below 25,000, the flow never reattaches at this low turbulence condition. These definitions were found to agree well with separation and reattachment locations derived from measured mean velocity profiles previously documented [8].

The effect of the chord Reynolds number can be seen by a direct comparison of the boundary layer profiles (measured via LDV) for the three Reynolds numbers shown in Fig. 5. These are plotted in the blade coordinate frame with the wall-normal axis of each profile shown as the solid line. The intersection of the axis line with the blade surface marks the zero velocity origin. At the same streamwise location, the boundary layer is thicker at the lower Reynolds number ($Re_c = 50,000$). The flow separates near $x/C_x = 72\%$ for all of the Reynolds number cases, but the height and extent of the separation bubble decreases with increasing Reynolds number. The separation bubbles are indicated by the dashed lines. As indicated, the extent of the separation bubble ranged from 25 to 12.5% of the axial chord as the chord Reynolds number increased from 50,000 to 100,000.

Two grid turbulence generators were used to provide higher freestream turbulence intensities to document its effect on the separation and reattachment locations. The turbulence characteristics were documented and presented in detail in our previous paper [8].

An example of the effect of the freestream turbulence level on the flow separation characteristics is shown in Fig. 6 for $Re_c = 50,000$. This shows mean velocity profiles in the blade coordinate frame. The top plot is identical to the top plot in Fig. 5 and corresponds to the the lowest freestream turbulence level of $u'/U_\infty = 0.08\%$. The bottom plot corresponds to the highest freestream turbulence level of $u'/U_\infty = 2.85\%$ which is 36 times larger.

The higher turbulence level did not affect the separation location. It did, however, significantly reduce the height and chordwise extent of the separation bubble. Based on these mean velocity profiles and C_p distributions [8], the point of flow reattachment moved upstream from $x/C_x \approx 97.5\%$ for $u'/U_\infty = 0.08\%$ to $x/C_x = 90\%$ for $u'/U_\infty = 2.85\%$.

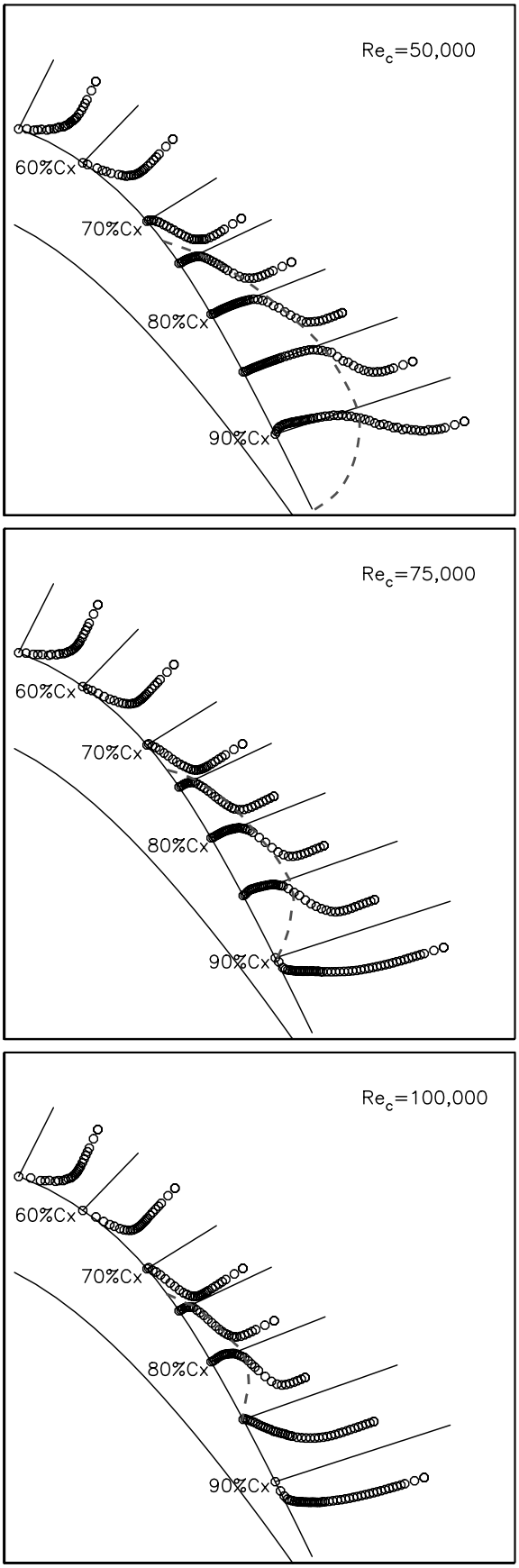

Fig. 5 Boundary layer profiles for three Reynolds numbers for lowest (0.08%) freestream turbulence intensity. The dashed lines sketch the extent of the separation bubble.

Based on the measured C_p distributions and boundary layer profiles, it is concluded that 1) the separation location is nearly independent of the chord Reynolds number and freestream turbulence level, with the nominal location being $x/C = 0.72$; 2) the reattachment location strongly depends on the chord Reynolds number, with the reattachment location decreasing as Re_c increases; and 3) the reattachment location is only slightly dependent on the freestream turbulence level, with the location decreasing as u'/U_∞ increases. For the range of Reynolds numbers up to and including 100,000, a separation zone is always present on the suction side of the blade regardless of the turbulence level.

B. Plasma Actuators

SDB plasma actuators consist of two electrodes that are separated by a dielectric material. One of the electrodes is typically exposed to the air. The other electrode is fully covered by the dielectric material. A schematic illustration is shown in Fig. 7. A high voltage ac potential is supplied to the electrodes. When the ac amplitude is large

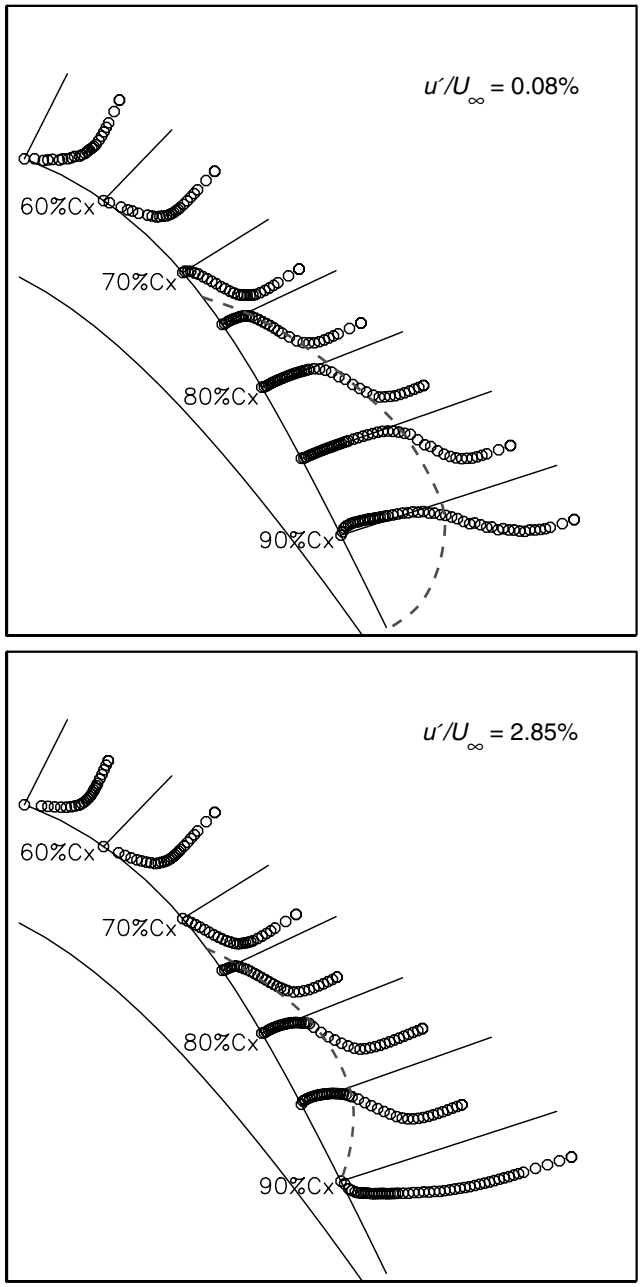

Fig. 6 Boundary layer profiles on PakB blades for two different freestream turbulence intensities at $Re_c = 50,000$.

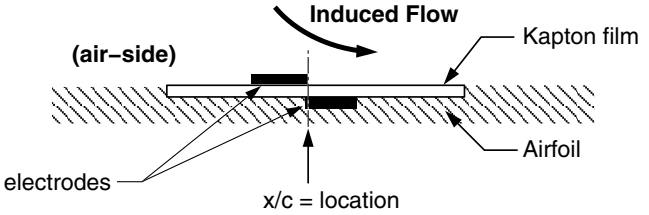

Fig. 7 Schematic drawing of asymmetric electrode arrangement for plasma actuators used in experiments.

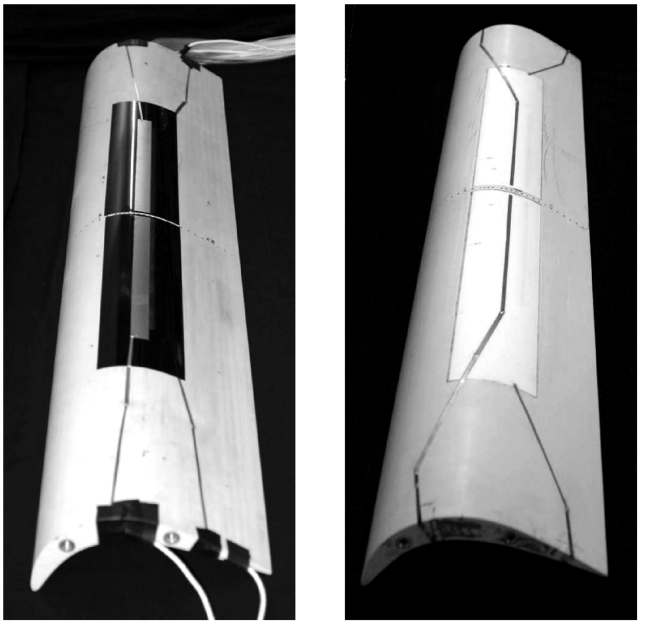

Fig. 8 Pictures of plasma actuators applied to PakB blades. Left used Kapton dielectric, right used Macor dielectric.

enough, the air ionizes in the region of the largest electric potential. This generally begins at the edge of the electrode that is exposed to the air and spreads out over the area projected by the covered electrode.

The process of ionizing the air in this configuration is classically known as a single dielectric barrier discharge [16,25]. The ionized air (plasma) in the presence of an electric field gradient produces a body force on the ambient air [17], inducing a virtual aerodynamic shape that causes a change in the pressure distribution over the surface on which the actuator is placed. The air near the electrodes is weakly ionized, and there is little or no heating of the air.

The body force per volume of plasma is given as

$$\boldsymbol{f} = \rho \boldsymbol{E} = -\left(\frac{\epsilon_0}{\lambda_D^2}\right)\phi \boldsymbol{E} \tag{1}$$

A lumped circuit model representation of the SDB plasma actuator [16,26] has demonstrated that the plasma volume, which is proportional to the dissipated power, scales as the applied voltage to the 7/2-power. Post [20] has shown that the maximum velocity produced in an asymmetric electrode arrangement like that in Fig. 7 also varies as $V^{7/2}$, which confirms the mechanism of the actuator. Orlov and Corke [26] have also examined the effect of the ac frequency on the power and scale of the actuator, which can be used in optimizing its design.

In this work, copper foil tape was used to make actuator electrodes. The nominal thickness of copper tape is 0.025 mm (1 mil). For the dielectric layer, two different materials were used in this research: Kapton and Macor. Kapton has a relatively high dielectric strength of 200 kV/mm and a low dielectric constant (with a typical value of 3.0). It is available in thin flexible sheets that allow it to be easily formed over curved surfaces. However, the free-oxygen (ozone) created by the plasma will eventually degrade the Kapton, giving it a finite life.

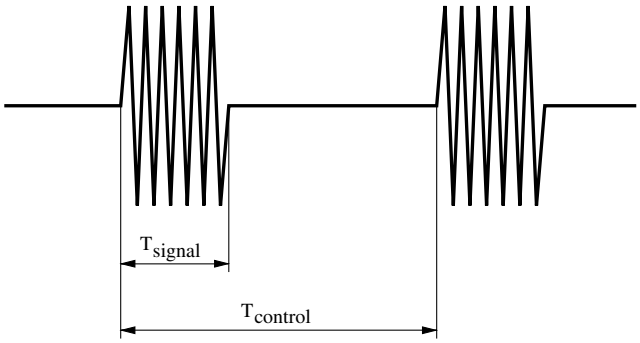

Fig. 9 The control signal sent to the plasma actuator during unsteady excitation.

Macor is a machinable ceramic. It has a lower dielectric strength (with a typical value of 40 kV/mm) and higher dielectric constant (with typical value of 6.0) than Kapton. The material is not flexible so that, except when used on a flat surface, it needs to be machined to shape. At typical voltage levels for the actuators, thicknesses of 0.008 to 0.010 in. are needed, which requires the actuators to be recessed into the surface to avoid passively disturbing the flow. Plasma actuators that use this material for the dielectric will operate indefinitely. Figure 8 shows photographs of both Kapton-based and Macor-based actuators as they were used with the PakB blades.

The electrodes were applied in the asymmetric arrangement that was illustrated in Fig. 7. They were overlapped by a small amount (on the order of 0.5 to 1 mm) to ensure a uniform plasma in the full spanwise direction.

The operating frequency of the ac voltage supplied to the electrodes was 5 kHz. This was primarily dictated by the electronics design and impedance matching considerations.

The ac voltage peak-to-peak amplitude to the electrodes ranged from 8 to 24 kV_{p-p}. The power required by the actuator varied depending on whether it was operated in a "steady" or unsteady mode. The steady mode is when the actuator is operated at the ac (on the order of 5 kHz) frequency. In many applications such as here, the flow does not respond to such high frequency disturbances so that the body force acting on the flow is effectively the time-averaged (steady) value.

In the unsteady mode of operation, the ac voltage was cycled off and on with an unsteady period. This is illustrated in Fig. 9 which shows a typical control signal that was sent to a plasma actuator during the unsteady excitation. Two important parameters of unsteady excitation are the excitation frequency and the plasma duty cycle defined in Eqs. (2) and (3), respectively.

$$f = \frac{1}{T_{\text{control}}} \tag{2}$$

$$\beta = \frac{T_{\text{signal}}}{T_{\text{control}}} \times 100\% \tag{3}$$

The choice of the unsteady frequency will be discussed in Sec. III. B.2.

1. *Steady Plasma Actuators*

In our previous work [8], steady plasma actuators were investigated. The approach was to use an asymmetric electrode design like that in Fig. 7 to produce a steady two-dimensional wall jet to energize the flow near the flow separation location. The wall jet produced by the actuator was oriented in the mean flow direction. From that study it was determined that 1) the optimum chordwise placement for the actuator is just upstream of the flow separation location, which on the blades is at $x/C = 0.7$; 2) there is a minimum actuator input amplitude below which there is no effect on the

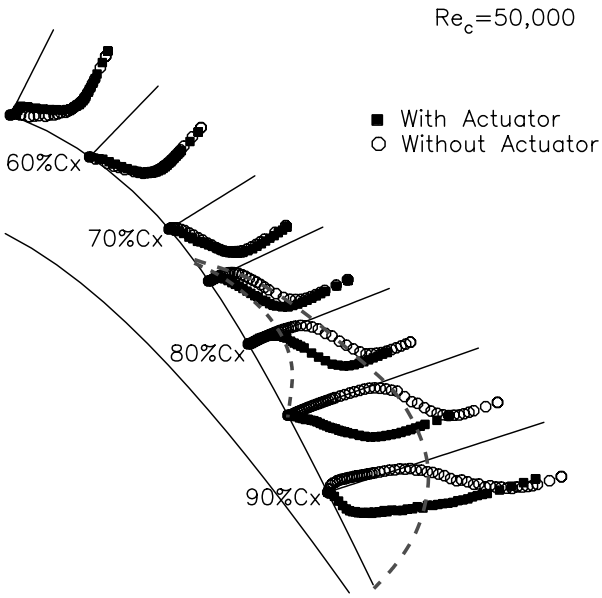

Fig. 10 The boundary layer profiles on a PakB blade with a single steady actuator operating and not operating at $Re_c = 50,000$.

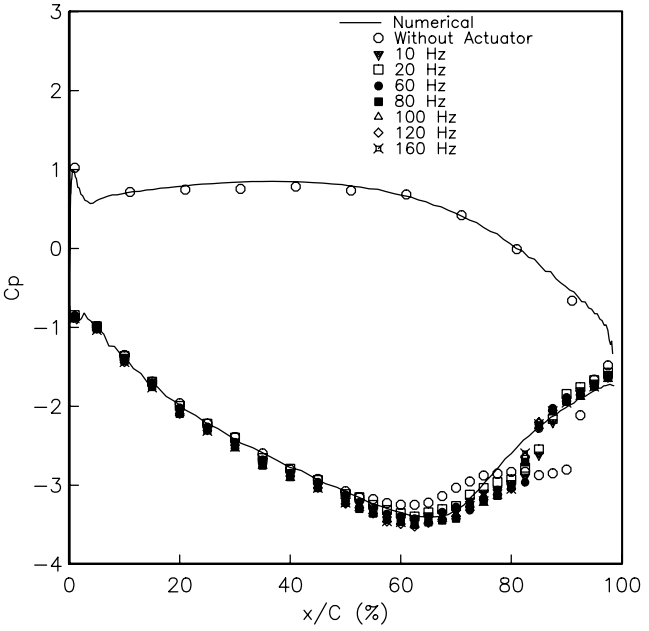

Fig. 11 Blade pressure distributions at $Re_c = 50,000$ for different excitation frequencies of an unsteady plasma actuator.

separated flow; 3) increasing voltages above the minimum threshold produces a proportional decrease in the size of the separation bubble, moving the reattachment point forward; 4) the effect of the actuator on the separation bubble eventually saturates, with further increases in the actuator amplitude showing no additional benefit.

An example of the effect of a single steady plasma actuator placed at $x/C_x = 67.5\%$ and operated at 8 kV is shown in Fig. 10. This presents mean velocity profiles (measured via LDV) over the suction side of the blade for $Re_c = 50,000$ at the lowest freestream turbulence level. The boundaries of the separation bubbles are sketched using dashed lines. The actuator is oriented to produce a wall jet in the mean flow direction.

At $x/C_x = 50\%$, the boundary layer profiles for the uncontrolled and controlled cases are not exactly the same as we would expect. This discrepancy was caused by the presence of the leading edge of the Kapton film, which produced a tiny step on the blade surface. Note that the effect of the tiny step is not evident by the next measurement location at $x/C_x = 60\%$.

The flow is separated at $x/C_x = 75\%$ for both uncontrolled and controlled cases. But in the controlled case, the extent of the separation bubble is much smaller. The plasma actuator caused the flow to reattach in this case by $x/C_x = 85\%$. With the actuator off, flow reattachment occurred at $x/C_x \geq 95\%$.

2. *Unsteady Plasma Actuators*

It has been shown in the literature that the introduction of unsteady disturbances near the separation location can cause the generation of large coherent vortical structures that could prevent or delay the onset of flow separation. These structures are thought to intermittently bring high momentum fluid to the surface, enabling the flow to withstand the adverse pressure gradient without separating. Periodic excitation by oscillatory blowing for use in separation control has been documented extensively by Seifert et al. [27,28] and in the review by Greenblatt and Wygnanski [29].

The forcing frequency for the unsteady disturbances is believed to be optimum when the Strouhal number $Sr = fL_{\text{sep}}/U_\infty$ is near unity. The local freestream velocity, in our case, corresponds to that in the midchannel between the blades $U_{\text{midchannel}}$. This is equivalent to requiring that the time scale for actuation match the time scale of the separated region.

This is consistent with the optimum Strouhal number if we substitute for the wavelength $\lambda = c/f$ in terms of the frequency, namely

$$Sr = fL_{\text{sep}}/U_\infty = \frac{cL}{\lambda U_\infty} = 1 \tag{4}$$

The nominal convection speed of a large-scale vortex in a boundary layer is $c = 0.5U_\infty$. Therefore, upon substitution

$$\lambda = 0.5L_{\text{sep}} \tag{5}$$

Based on this scaling, we expect two vortices in the separated region when excited by the unsteady actuator at $Sr = 1$.

A sensitivity study was performed to determine if such an optimum frequency existed for the unsteady actuator used in controlling the flow separation on the PakB blade. This involved operating the plasma actuator at different unsteady frequencies for the conditions of $Re_c = 50,000$ and the lowest freestream turbulence level. The design and placement of the actuator were identical to the steady operation described in the previous section. The results are summarized in Fig. 11, which shows the C_p distribution on the suction side of the blade for a range of unsteady actuator frequencies from 10 to 160 Hz. The actuator was located at $x/C_x = 67.5\%$. In all cases the duty cycle was 10%, which will be shown later to be a sufficient value.

As previously discussed, the deviation of the measured C_p values from the inviscid distribution, shown as the solid curve, is an indication of the flow separation zone. The pressure distributions in Fig. 11 indicate that the deviation decreases with increasing frequency. The question is if an optimum frequency exists.

To examine if an optimum frequency exists, the difference between the measured C_p values and the inviscid value at one location of $x/C_x = 85\%$ (in the separated flow region) was plotted versus the excitation frequency. The result is shown in Fig. 12. Note in the figure, the excitation frequency has been converted into a Strouhal number defined as

$$Sr \equiv \frac{fL_{\text{sep}}}{U_{\text{midchannel}}} \tag{6}$$

At $Re_c = 50,000$, $U_{\text{midchannel}} \approx 9.4$ m/s, and the separation zone is from $x/C_x = 72.5$ to 97.5% giving $L_{\text{sep}} = 3.25$ in. (8.26 cm). Therefore, for $Sr = 1$, $f = 114$ Hz.

The unsteady actuator effectiveness improves as the difference between the measured C_p values and the inviscid value decreases. In Fig. 12 a rapid improvement occurs as the unsteady excitation frequency increases. This reaches an optimum improvement very close to the frequency corresponding to $Sr = 1$, which is shown as

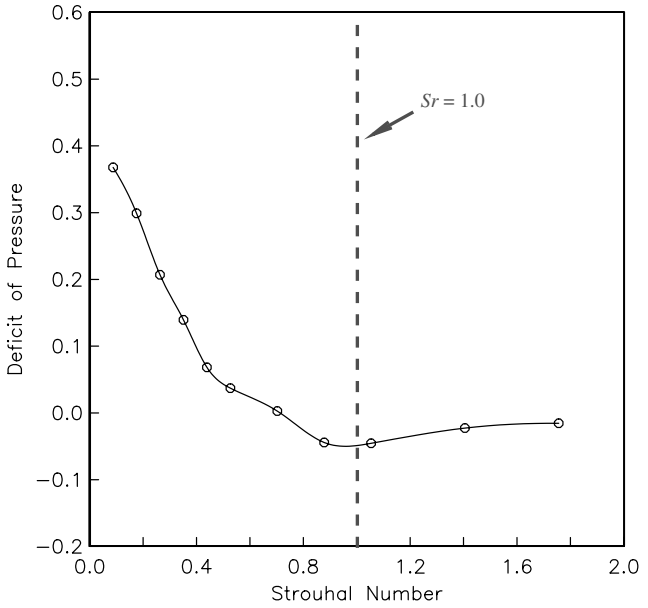

Fig. 12 Difference between measured C_p values and inviscid value at $x/C_x = 85\%$ for different excitation frequencies at $Re_c = 50,000$.

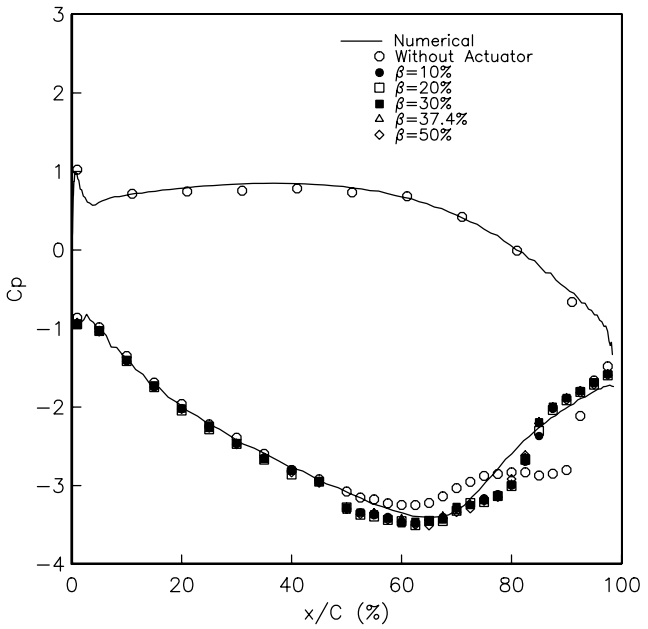

Fig. 13 C_p distributions at $Re_c = 50,000$ for different unsteady plasma actuator duty cycles at $Sr = 0.4$.

the dashed line in the figure. Higher frequencies above the optimum value do not appear to severely degrade the performance of the actuator to reattach the flow. However, there will be an actuator input power disadvantage.

Another important parameter for the unsteady actuator control is the duty cycle, especially since a lower duty cycle can reduce the average power used by the actuator. Bons et al. [6] studied the effect of the duty cycle when using the pulsed jets to control turbine blade separation. They found that the unsteady jets were still effective even when a duty cycle as low as 1% was used.

The effect of the duty cycle for plasma actuators is presented in Fig. 13. This corresponds to $Re_c = 50,000$ and the lowest freestream turbulence level. The unsteady actuator frequency was 40 Hz which corresponds to $Sr = 0.4$, and the actuator was located at $x/C_x = 67.5\%$. From Fig. 12 this produced approximately 80% of the improvement reached at the optimum frequency. The C_p distributions for duty cycles from 50 to 10% are presented. These

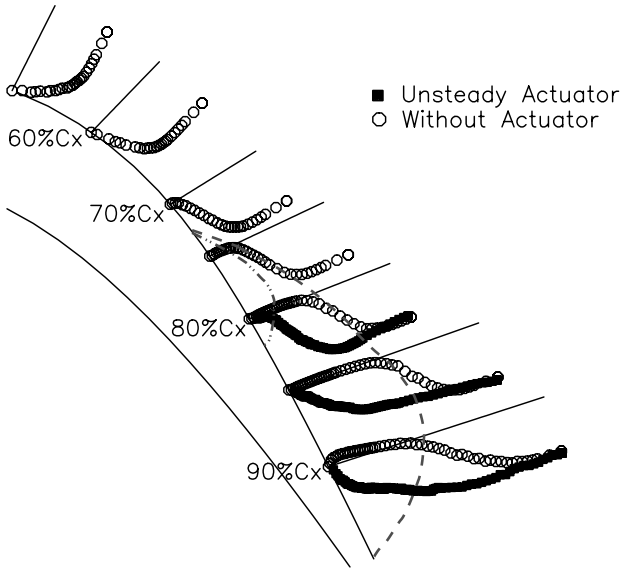

Fig. 14 The boundary layer profiles with an unsteady actuator operating $Sr = 0.9$ and not operating, for $Re_c = 50,000$. Separation bubbles are sketched using dashed lines.

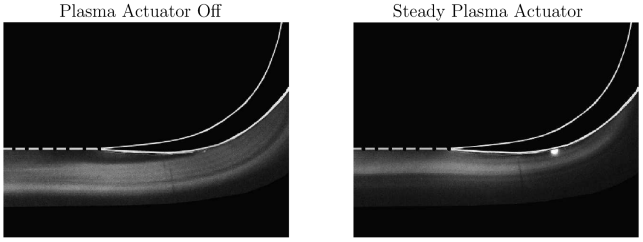

Fig. 15 Flow visualization records on PakB blade suction side at $Re_c = 25,000$.

indicate that the lowest duty cycle of 10% was as effective as the highest duty cycle. Therefore, this offers a 400% power reduction for the same actuator effectiveness.

The mean velocity profiles on the suction side of the blade were measured using a constant-current hot-wire probe that was specifically designed [9] to examine the effects of the unsteady plasma actuators. These are shown in the blade coordinate frame by the closed symbols in Fig. 14 for $Re_c = 50,000$. The unsteady actuator frequency is close to the optimum and the duty cycle is 10%.

The unsteady actuator caused the flow to be reattached at $x/C_x = 80\%$. At the same location for the steady actuator, the flow was still separated as seen in the mean velocity profiles in Fig. 14. Thus, the unsteady actuator was more effective. The reasons for this will be discussed in the Sec. III.C.

C. Mechanism of Plasma Actuator Separation Control

A single plasma actuator placed just upstream of the flow separation location proved to be effective in causing the flow to reattach on the suction side of the PakB blade. The effect of the steady actuator was found to be asymptotic with increasing input amplitude and was unable to eliminate the separation bubble completely. The unsteady actuator was able to eliminate the separation bubble and at the lower duty cycle accomplished this at one-tenth the power of the steady actuator. The question is what are the mechanisms behind the two modes of operation that differentiates their effectiveness?

1. Steady Plasma Actuator

As a first step in answering this question, we consider flow visualization. An example of the flow over the suction side of the

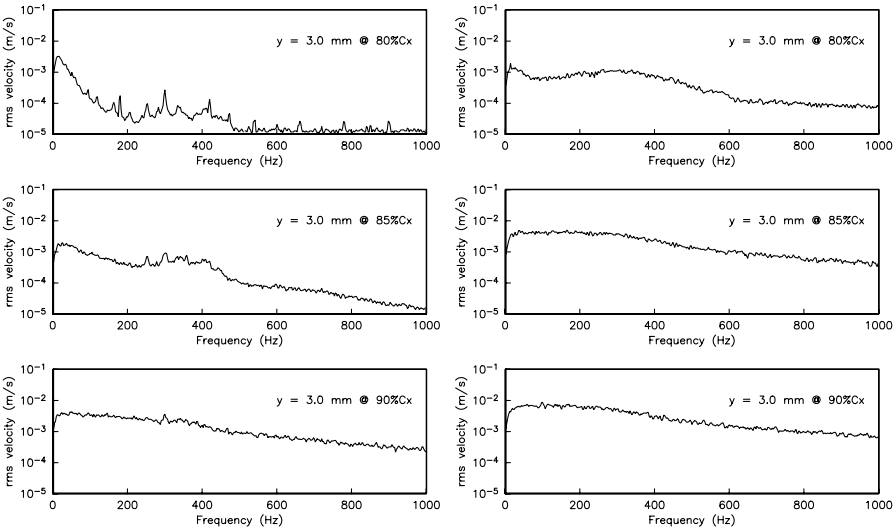

Fig. 16 Velocity spectra at three streamwise locations for base flow (left) and with steady plasma actuator. $Re_c = 50,000$.

blade at $Re_c = 25,000$ is shown in Fig. 15. The flow direction is from right to left, and the images show the trailing-edge portion of the blade. The left photograph corresponds to the base flow over the suction side of the blade with the actuator off. The right photograph corresponds to the flow with a steady actuator. The plasma actuator location, $x/C_x = 67.5\%$, is visible as the bright spot in the image at the surface of the blade.

As presented earlier, the basic flow separates at $x/C_x \approx 72\%$. At the Reynolds number in the image and the low turbulence condition, the flow does not reattach on the blade. The separation zone appears as the dark region near the trailing edge of the blade. The outer flow and attached flow upstream of the separation location appear white.

When the steady actuator is on, the flow appears to be attached and leaves the blade tangent to the trailing edge. Surface pressure measurements and mean velocity profiles [9] had indicated that the flow reattached in this case at $x/C_x \approx 85\%$. On close inspection of the flow visualization image, we can observe a dark region immediately downstream of the actuator that extends approximately half the distance to the trailing edge. This would correspond to $x/C_x \approx 86\%$, which is consistent with the quantitative measurements.

To understand more about the mechanism of flow reattachment for the plasma actuators, the spectra of velocity fluctuations were measured using a hot wire. These are presented in Fig. 16 for three locations of $x/C_x = 80$, 85, and 90% at a representative fixed height above the surface of the blade at $Re_c = 50,000$. At $x/C_x = 80\%$, the measurement height corresponds to $y/\delta \simeq 0.6$. The left column of spectra correspond to the base flow with the actuator off. The right column corresponds to when the steady plasma actuator was operating.

For the base flow, as was shown in the C_p distributions at this Reynolds number in Fig. 4, the flow reattached at $x/C_x \simeq 95\%$. Upstream of that location at $x/C_x = 80\%$, the spectra indicate a large amount of low frequency unsteadiness, as well as a broad peak centered at approximately 300 Hz. The low frequency is somewhat intrinsic to separation bubbles. The 300 Hz peak is likely associated with the Kelvin–Helmholtz instability of the separated shear layer. A little farther downstream at $x/C_x = 85\%$, fluctuations in broadband frequencies are beginning to fill the spectrum. By $x/C_x = 90\%$, where the flow is reattaching, the spectrum has a broadband character that is indicative of a turbulent boundary layer. On the basis of the spectra, the flow reattachment appears to be the result of turbulent transition of the separated shear layer.

For the case with the steady plasma actuator, Fig. 10 indicated that the flow reattached at $x/C_x = 85\%$. Upstream of that location at $x/C_x = 80\%$, the spectra show a broad peak centered about 300 Hz that we associated with the shear layer instability, as well as a large amount of broadband spectral filling. Farther downstream, $x/C_x \geq 85\%$, where the flow was determined to reattach, the spectra have the same broadband character of a turbulent boundary layer. The steady plasma actuator has accelerated the process of flow reattachment, with the attached flow having the same spectral character as the natural reattached flow.

Based on the spectra, we surmised that the steady plasma actuator acted like a turbulence "trip." To test this assumption, different designs of the actuator were tried [9]. In addition to the design used in all of the previous results, in which the actuator induces a steady jet along the surface in the mean flow direction, alternate designs that induced an upstream oriented wall jet and simultaneous upstream and downstream wall jets were investigated. The results for these were comparable thereby supporting the assumption that the steady plasma actuator acted like a trip in causing the flow to reattach.

2. *Unsteady Plasma Actuator*

To understand the mechanism behind the unsteady plasma actuators, we again started with flow visualization. A sample of these is shown in Fig. 17. This shows three consecutive frames from a video where the unsteady actuator was operating at 20 Hz and the laser light sheet used to illuminate the visualization particles was chopped at 21 Hz to produce a difference frequency of 1 Hz. The Reynolds number was 25,000 so that the flow visualization can be directly compared with the images in Fig. 15.

The principle behind the use of the unsteady plasma actuator was to generate spanwise vortices that could bring high momentum fluid towards the blade surface. Although the flow visualization cannot provide quantitative evidence of spanwise vortices, we can observe periodic features that are being convected downstream of the actuator. These appear as dark regions over the surface of the blade. The top image in Fig. 17 shows this dark feature just downstream of the actuator on the blade surface. The middle image is 1/30 s later. This shows the dark feature moved to near the trailing edge of the blade. In the last image in the sequence, the dark feature is off the end of the blade. Accounting for the time difference between images, the convection speed can be estimated to be

$$U_c = \frac{\Delta x}{\Delta t} = 2.33 \text{ m/s} \tag{7}$$

The local freestream velocity at $Re_c = 25,000$ was 4.7 m/s. Therefore, the convection velocity of these features was almost half of the midchannel velocity ($0.5U_{\text{midchannel}}$), which is the expected convection speed for spanwise vortices.

Aside from the convected features in the images, the flow appears to follow the blade surface without any indication of a flow separation. This is readily seen by comparing, for example, the bottom image with those in Fig. 15. In particular, in terms of the flow

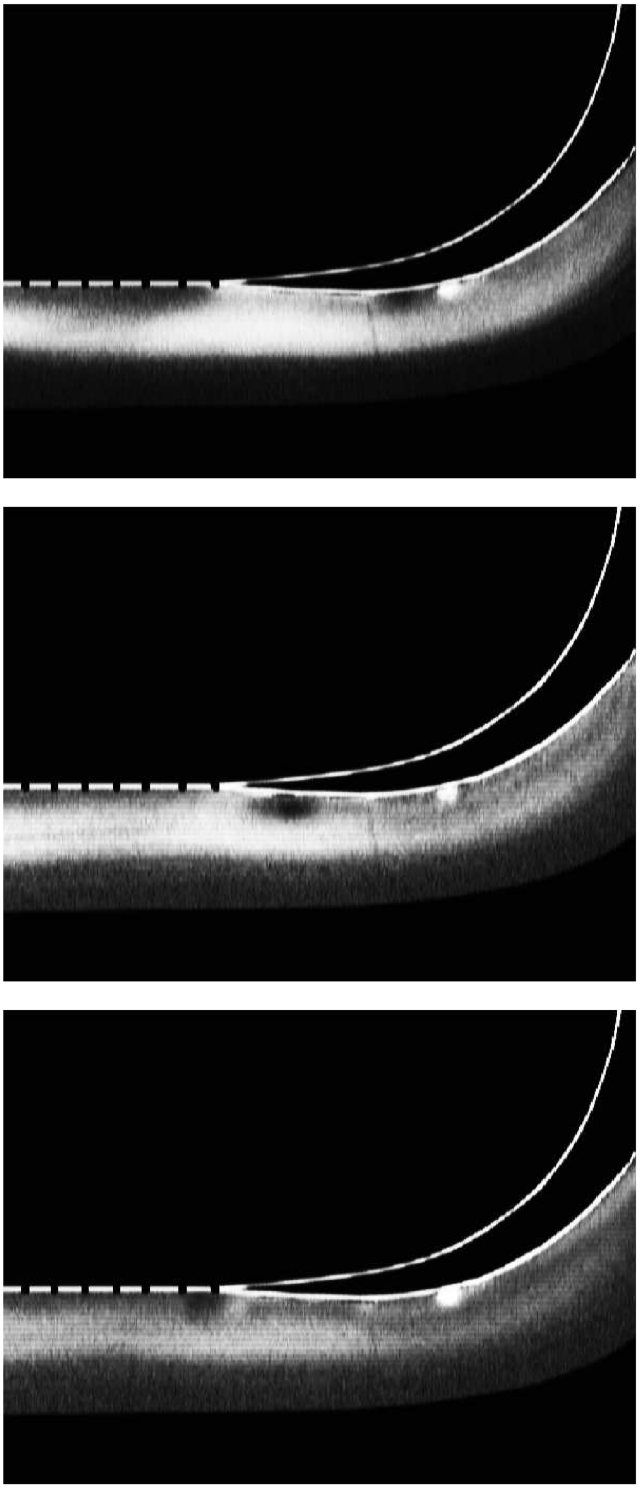

Fig. 17 Consecutive video frames showing the effect of unsteady plasma actuator at $Sr = 0.4$. $Re_c = 25,000$.

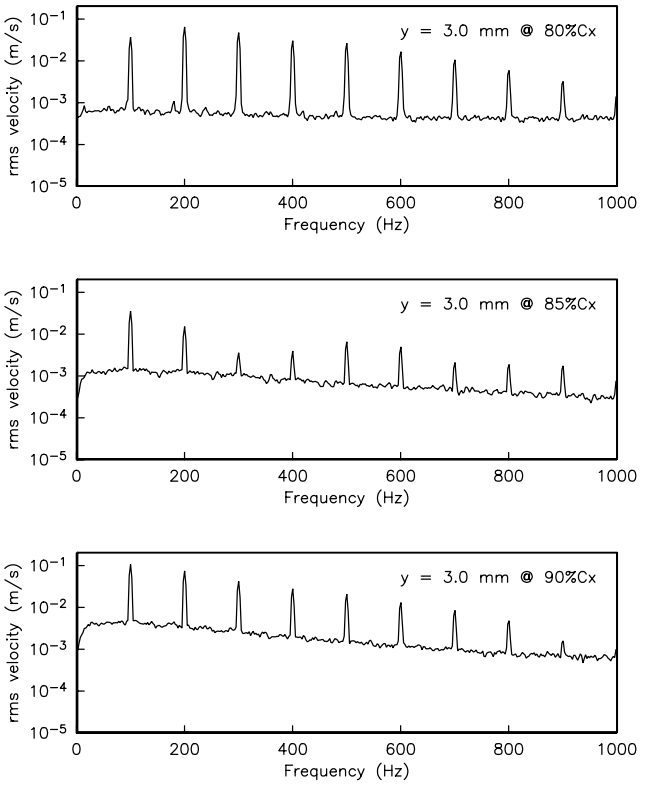

Fig. 18 Velocity spectra at three streamwise locations with unsteady plasma actuator frequency at $Sr = 0.9$.

attachment as evidenced by the flow visualization, the unsteady actuator is markedly better than the steady actuator. As pointed out earlier, a similar conclusion was made by Bons et al. [6].

Figure 18 shows velocity spectra at three streamwise locations for the unsteady actuator at $Re_c = 50,000$. The actuator frequency is close to the optimum at 100 Hz ($Sr = 0.9$). For reference, these spectra can be directly compared with those for the base flow and steady actuator that were shown in Fig. 16.

The velocity spectra for the flow with the unsteady plasma actuator display two important features. The first is the large spectral peaks at the unsteady excitation frequency and higher harmonics. Special steps were taken [9] to ensure that these peaks were not due to electronic noise but were actually due to the unsteady flow field generated by the plasma actuator. The second important feature is the high level of the background fluctuations that are comparable to those with the steady actuator after the flow reattached. The combination of these two features suggests that the unsteady actuator is producing a strong periodic flow structure that rapidly leads to turbulent mixing of the flow.

D. Loss Coefficient

The overall study was largely motivated by the larger than predicted loss coefficients of LPT blades found by Sharma [1]. We, therefore, compared in our experiment the loss coefficients for the base flow condition at different Reynolds numbers and the improvement that came about with the unsteady plasma actuator. The loss coefficient η was defined as

$$\eta \equiv \int \frac{p_{0_{ds}} - p_{0_{us}}}{\frac{1}{2}\rho U_\infty^2}\,\mathrm{d}y \tag{8}$$

where $p_{0_{us}}$, which is the total pressure, and U_∞ are both measured upstream of the cascade and $p_{0_{ds}}$ is the total pressure measured downstream in the blade wake.

An example of spanwise profiles of the mean velocity in the wakes of the blades at $Re_c = 25,000$ is shown in Fig. 19. These were measured at $0.5C_x$ downstream of the cascade. The spanwise extent of the profiles covers two blade spacings. The position of the blade with the plasma actuator is at $y/y_{\text{blade}} = 1.5$ in the figure. The profile with the square symbols corresponds to the base flow. The velocities have been normalized by the largest midchannel velocity in the base flow. In this case, the wakes of the consecutive blades are clearly visible as the largest velocity deficits.

The profile with the circle symbols corresponds to the case with the plasma actuator operating. The plasma actuator significantly reduces the velocity deficit. In addition the wake width is significantly reduced, and the location of the velocity minimum is

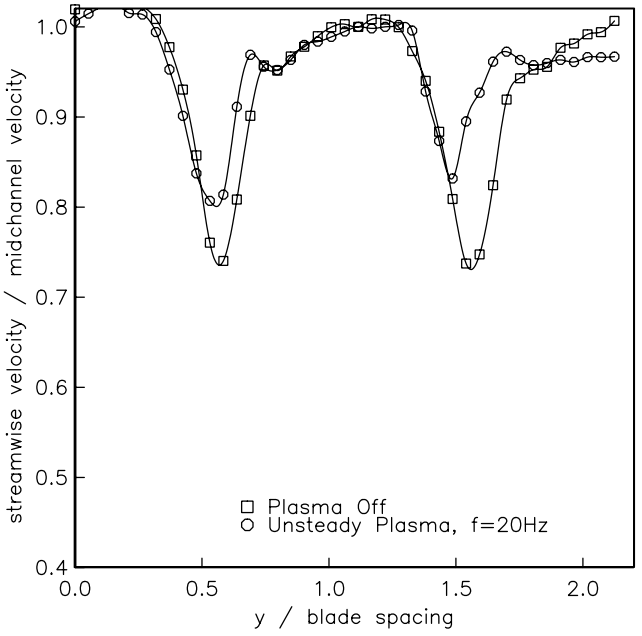

Fig. 19 Spanwise profiles of the mean velocity measured $0.5C_x$ downstream of the cascade for base flow and with an unsteady plasma actuator located on the blade at $y/y_{\text{blade}} = 1.5$. $Re_c = 25,000$.

shifted. The movement of the velocity minimum reflects a change in the mean velocity vector to become tangent to the trailing edge. This was not the case with the actuator off as was evident in the flow visualization in Fig. 15.

We also note that although the plasma actuator was located on only one blade, whose wake is at $y/y_{\text{blade}} = 1.5$, it had an effect on the adjacent blade, whose wake is at $y/y_{\text{blade}} = 0.5$ and is significantly narrower. We believe this effect is due to the added turning of the flow on the blade with the actuator that produced a more favorable condition on other blades in the cascade. In a similar experiment by Bons et al. [4], pulsing vortex generator jets used to control separation on PakB blades also narrowed the wake of the controlled blade but broadened the wake of the next blade. Our result is more favorable.

Based on Eq. (8), the wake profile of the blade with the actuator was used to calculate the total pressure loss coefficient. The results are shown in Fig. 20 for two Reynolds numbers. At the lowest Reynolds number, the base flow was fully separated from the blade. The contrast between that state and the fully attached state produced by the plasma actuator was significant and resulted in a 200% reduction in the loss coefficient.

The improvement in the loss coefficient at $Re_c = 50,000$ was not as significant. The reason is that, at this Reynolds number, the base flow separated but reattached before the blade trailing edge. The result was that the losses in the wake were not as significant. Consequently, the contrast between the base flow state and the fully attached state produced by the actuator were not as large so that the gains to be made were smaller. In this case, a 22% improvement in the loss coefficient was obtained. At higher Reynolds numbers, the improvements will be smaller.

IV. Summary

Active boundary layer separation control has been successfully demonstrated on a LPT blade using plasma actuators. The experiments were performed in a specially designed wind tunnel that hosts a generic LPT cascade consisting of nine PakB blades. The flow fields around PakB blades with and without separation control were thoroughly documented using flow visualization, pressure measurements, LDV measurements, and hot-wire measurements.

The experimental conditions were chosen to give a range of chord Reynolds numbers from 10,000 to 1000,000 and a range of the freestream turbulence intensities from $u'/U_\infty = 0.08$ to 2.85%. For

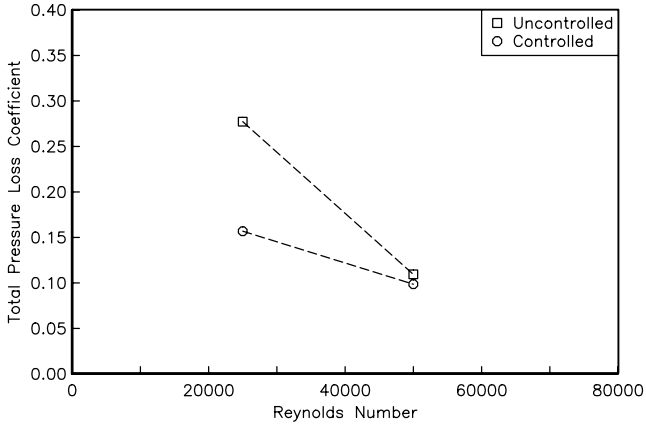

Fig. 20 Total pressure loss coefficients at two Reynolds numbers for the base flow and with an unsteady plasma actuator.

the range of conditions studied, the separation location was nearly independent on the chord Reynolds number and freestream turbulence intensity. The nominal location was at $x/C_x = 72\%$. The location of reattachment was found to be strongly dependent on the chord Reynolds number and slightly dependent on the turbulence intensity. In all cases, some separation region existed. At the lower chord Reynolds numbers, $Re_c < 50,000$, at all but the highest turbulence intensity, the flow never reattached. Even at the highest Reynolds numbers and turbulence intensities, a separation zone was always present on the suction side of the blade.

Plasma actuators were designed and applied to control the flow separation occurring on the suction surface of the PakB blade. Both steady and unsteady actuation were implemented and found to be effective at separation control. The steady plasma actuator was the most effective when applied sightly upstream of the separation location. The amplitude of the steady plasma actuators had a minimum threshold value to produce an effect on the flow separation. In addition, the effect of the steady actuator saturated at larger amplitudes. The control mechanism of the steady actuators was suggested to be turbulence tripping of the laminar separation flow. For the unsteady actuators, there exists an optimum excitation frequency. This optimum frequency is the one that makes the Strouhal number, defined as $Sr = fL_{\text{sep}}/U_{\text{midchannel}}$, unity. The lowest plasma duty cycle (10%) was as effective as the highest plasma duty cycle (50%) at the same excitation frequency. Both flow visualization and the power spectra show that the control mechanism of the unsteady actuators is the generation of spanwise flow structures that promote mixing.

Acknowledgments

This work was supported by a Cooperative Agreement with the NASA Glenn Research Center number NCC3-775 and monitored by David Ashpis.

References

[1] Sharma, O., "Impact of Reynolds Number on Low Pressure Turbine Performance," NASA CP-1998-206958, 1998, pp. 65–69.

[2] Byerley, A. R., Störmer, O., Baughn, J. W., Simon, T. W., Van Treuren, K. W., and List, J., "Using Gurney Flaps to Control Laminar Separation on Linear Cascade Blades," American Society of Mechanical Engineers Paper GT-2002-30662, 2002.

[3] Lake, J. P., King, P. I., and Rivir, R. B., "Reduction of Separation Losses on a Turbine Blade with Low Reynolds Number," AIAA Paper 1999-0242, 1999.

[4] Bons, J. P., Sondergaard, R., and Rivir, R. B., "Control of Low Pressure Turbine Separation Using Vortex Generator Jets," AIAA Paper 1999-0367, 1999.

[5] Bons, J. P., Sondergaard, R., and Rivir, R. B., "Turbine Separation Control Using Pulsed Vortex Generator Jets," *Transactions of the ASME: Journal of Turbomachinery*, Vol. 123, April 2001, pp. 198–206.

[6] Bons, J. P., Sondergaard, R., and Rivir, R. B., "The Fluid Dynamics of

LPT Blade Separation Control Using Pulsed Jets," *Transactions of the ASME: Journal of Turbomachinery*, Vol. 124, Jan. 2002, pp. 77–85
[7] Volino, R. J., "Separation Control on Low Pressure Turbine Airfoils Using Synthetic Vortex Generator Jets," *Transactions of the ASME: Journal of Turbomachinery*, Vol. 125, No. 4, 2003, pp. 765–777.
[8] Huang, J., Corke, T. C., and Thomas, F. O., "Plasma Actuators for Separation Control of Low Pressure Turbine Blades," AIAA Paper 2003-1027, 2003.
[9] Huang, J., "Documentation and Control of Flow Separation on a Linear Cascade of Pak-B Blades Using Plasma Actuators," Ph.D. Dissertation, University of Notre Dame, Notre Dame, IN, April 2005.
[10] Orlov, D., Erturk, E., Post, M., and Corke, T., "DNS Modeling of Plasma Array Flow Actuators," *Bulletin of the American Physical Society Fluid Dynamics Division*, Vol. 46, No. 10, 2001, p. 217.
[11] Corke, T. C., and Matlis, E., "Phased Plasma Arrays for Unsteady Flow Control," AIAA Paper 2000-2323, 2000.
[12] Post, M. L. "Phased plasma actuators for unsteady flow control," M.S. thesis, University of Notre Dame, Notre Dame, IN, 2001.
[13] Matlis, E., "Controlled Experiments on Instabilities and Transition to Turbulence on a Sharp Cone at Mach 3.5," Ph.D. Dissertation, University of Notre Dame, Notre Dame, IN, 2003.
[14] Corke, T. C., Jumper, E. J., Post, M. L., Orlov, D., and McLaughlin, T. E., "Application of Weakly-Ionized Plasmas as Wing Flow Control Devices," AIAA Paper 2002-0350, 2003.
[15] Wilkinson, S. P., "Investigation of an Oscillating Surface Plasma for Turbulent Drag Reduction," AIAA Paper 2003-1023, 2003.
[16] Enloe, C. L., McLaughlin, T. E., VanDyken, R. D., Kachner, K. D., Jumper, E. J., and Corke, T. C., "Mechanisms and Responses of a Single Dielectric Barrier Plasma Actuator: Plasma Morphology," *AIAA Journal*, Vol. 42, March 2004, pp. 589–594.
[17] Enloe, L., McLaughlin, T., VanDyken, R., Kachner, K., Jumper, E., and Corke, T., "Mechanisms and Response of a Single Dielectric Barrier Plasma Actuator: Plasma Morphology," *AIAA Journal*, Vol. 42, No. 3, March 2004, pp. 589–594.
[18] Post, M., and Corke, T., "Separation Control on High Angle of Attack Airfoil Using Plasma Actuators, *AIAA Journal*, Vol. 42, No. 11, 2004, pp. 2177.
[19] Corke, T. C., He, C., and Patel, M. P., "Plasma Flaps and Slats: An Application of Weakly-Ionized Plasma Actuators," AIAA Paper 2004-2127, 2004.
[20] Post, M. L., "Phased Plasma Actuators for Separation Control on Stationary and Oscillating Airfoils," Ph.D. Dissertation, University of Notre Dame, Notre Dame, IN, 2004.
[21] Thomas, F. O., Koslov, A., and Corke, T. C., "Plasma Actuators for Landing Gear Noise Reduction," AIAA Paper 2005-3010, 2005.
[22] Hultgren, L. S., and Ashpis, D. E., "Demonstration of Separation Delay with Glow Discharge Plasma Actuators," AIAA Paper 2003-1025, 2003.
[23] Corke, T. C., and Post, M. L., "Overview of Plasma Flow Control: Concepts, Optimization, and Applications," AIAA Paper 2005-0563, 2005.
[24] Figliola, R. S., and Beasley, D. E., *Theory and Design for Mechanical Measurements*, Wiley, New York, 1991.
[25] Fridman, A., and Kennedy, L., *Plasma Physics and Engineering*, Taylor and Francis, Philadelphia, PA, 2004.
[26] Orlov, D., and Corke, T. C., "Numerical Simulation of Aerodynamic Plasma Actuator Effects," AIAA Paper 2005-1083, 2005.
[27] Seifert, A., Bachar, T., Moss, D., Shepshelovish, M., and Wygnanski, I., "Oscillatory Blowing: A Tool to Delay Boundary-Layer Separation," *AIAA Journal*, Vol. 11, No. 31, 1993, pp. 2052–2060.
[28] Seifert, A., Darabi, A., and Wygnanski, I., "Delay of Airfoil Stall by Periodic Excitation," *Journal of Aircraft*, Vol. 33, No. 4, 1996, pp. 691–698.
[29] Greenblatt, D., and Wygnanski, I., "The Control of Separation by Period Excitation," *Progress in Aerospace Sciences*, Vol. 36, 2000, pp. 487–545.

M. Auweter-Kurtz
Associate Editor